International Conference on Computational Methods in Marine Engineering
MARINE 2011
L.Eça, E. Oñate, J. García, T. Kvamsdal and P. Bergan (Eds)

EXPLORATORY RANS SIMULATIONS OF PARTIAL CAVITATION AND ITS DYNAMICS

MARTIN HOEKSTRA*

* Maritime Research Institute Netherlands (MARIN)
Wageningen, The Netherlands
e-mail: m.hoekstra@marin.nl

Key words: Computational Fluid Dynamics, Cavitation, NACA0015.

Summary. Partial cavitation on a 2D foil at given incidence goes through various stages when the cavitation number is lowered. This paper explores by numerical simulation the transition from more or less steady to dynamic behaviour, eventually leading to periodic shedding of vapour clouds. Cavitation modeling is in this paper based upon the single, variable-density fluid approach, solving the RANS equations with the k-ω SST turbulence model and the Sauer/Schnerr mass transfer model. Results are presented for the NACA0015 foil at six degrees incidence. Effects of spatial and temporal resolution are included in the investigation. When shedding of vapour clouds occurs, the results clearly show that it is accompanied with dynamic stall behaviour, *i.e.* the flow on the suction side of the foil is intermittently separated and attached.

1 INTRODUCTION

This paper descibes a numerical study of cavitation in the two-dimensional flow over a foil at a fixed angle-of-attack. Numerical simulation of cavitation has for a long time been based exclusively on potential flow models. During the last two decades, however, the preferred model has for many researchers changed to RANS, DES or LES, with the prospect of more realism in the simulations. But such enhanced realism has of course to be shown and substantiated. Solving RANS equations for a single, variable-density fluid, the author has studied the cavitation behaviour of a 2D NACA0015 foil at 6 degrees angle-of-attack. Results for the steady regime have been published earlier[1], while a critical examination of the re-entrant jet flow - widely accepted as the cause of instability and cloud shedding - appeared recently as a follow-up [2]. Experiments indicate that, even on a stationary foil in a steady and uniform inflow, the cavity can get in a dynamic state. This intrinsic instability locks in to a periodic behaviour, eventually including the regular shedding of vapour clouds. In this paper the focus is on the numerical reproduction of this transition from stationary to dynamic cavitation. Does the instability appear in the numerical simulation? If so, do the results give a clue to the origin of the instability? Why does the flow become periodic instead of chaotic? These questions will be addressed after a brief introduction of the mathematical model and the computational settings. Illustrative results will be presented.

2 MATHEMATICAL MODEL

When the pressure in a liquid drops below the saturated vapour pressure at the prevailing temperature, the liquid gets in an unstable state and normally tends to form vapour pockets. The fluid is then locally either in liquid or in vapour state, if the presence of non-condensable gas is neglected, and we can deservedly speak of a two-phase flow. However, on the scale of a grid cell in a typical RANS simulation, the fluid may also be said to be in a mixed state, *i.e.* small regions exist which are nevertheless big enough to be partly filled with liquid, partly with vapour. In the mathematical model used in this paper we go one step further by assuming that the continuum hypothesis still applies. Thus we deal with cavitating flows by solving continuum equations for a single, variable-density fluid, the density ρ being linked to the vapour volume fraction α_v by

$$\rho = (1-\alpha_v)\rho_l + \alpha_v\rho_v \tag{1}$$

where the densities of liquid (ρ_l) and vapour (ρ_v) are assumed to be constants. In other words, the fluid may be water or vapour or a uniform mixture of both. It means that no discontinuous changes occur in the density, nor in any of the other variables, and that the liquid-vapour interface is never perfectly sharp. This is in contrast with potential-flow models for cavitating flows but at the same time not altogether unrealistic. Indeed, strict adherence to a sharp interface leads inevitably to conflicts. They are avoided in the single-fluid approach: there is no flow detachment paradox at the front end of a partial cavity, nor is there a mass balance problem as in the case of the re-entrant jet flow model [2]. Moreover, in our approach no restrictions are imposed on the topology of the cavity, thereby allowing break-up of the cavity and shedding of vapour clouds.

Taking the single-fluid approach as a starting point, we adopt the RANS equations with the k-ω SST turbulence model to control mass and momentum conservation. The molecular viscosity of the fluid is, like the density, assumed to be linearly dependent on α_v. Compared to RANS for an incompressible fluid, the density is an extra variable, hence an extra equation is required to close the system. This is the evaporation/condensation model, in our case a transport equation for the vapour volume fraction with a source/sink term

$$\frac{\partial \alpha_v}{\partial t} + \nabla . \alpha_v \bar{u} = \frac{S}{\rho_v}, \tag{2}$$

in which the source term follows the proposal of Sauer/Schnerr [3, 4] and is here written as

$$\frac{S}{\rho_v} = 3(\tfrac{4}{3}\pi n_0)^{1/3}(1-\alpha_v)^{1/3}\alpha_v^{\,2/3} sign(p_v - p)\sqrt{\frac{2}{3}\frac{|p_v - p|}{\rho_l}}. \tag{3}$$

The properties of this source term have been discussed by Hoekstra & Vaz [1]. For later reference we give here the relation between source term and rate of expansion

$$\frac{S}{\rho_v} = \frac{\rho_l}{\rho_l - \rho_v}\nabla . \bar{u} \tag{4}$$

and recall that the time rate of change of the total vapour volume equals the source integral

$$\frac{d}{dt}\int \alpha_v dV = \int \frac{S}{\rho_v} dV \tag{5}$$

The single free parameter of the source term, the number of nuclei per unit of volume n_0, has been set in all computations presented in this paper at $n_0 = 10^8$. Its sole function is to modulate the rate of evaporation and condensation.

Some remarks are in place here on the application of RANS to unsteady flows. The RANS equations are derived from the Navier-Stokes equations by time averaging, giving the Reynolds stresses as a by-product. A turbulence model is needed to account (approximately) for the effect of these Reynolds stresses on the mean flow. Time-derivatives disappear, and from the velocity, decomposed in a time-mean and a fluctuating component as:

$$\overline{U}(\bar{x},t) = \bar{u}(\bar{x}) + \bar{u}''(\bar{x},t) \tag{6}$$

the time-averaged part $\bar{u}$ is computed, while the fluctuating component $\bar{u}''$ is not evaluated explicitly.

But if the time-derivatives are maintained and a RANS simulation produces a velocity varying in time, denoted as $\bar{\tilde{u}}(\bar{x},t)$, we have

$$\overline{U}(\bar{x},t) = \bar{\tilde{u}}(\bar{x},t) + \bar{u}''(\bar{x},t) = \bar{u}(\bar{x}) + \bar{u}'(\bar{x},t) + \bar{u}''(\bar{x},t) \tag{7}$$

and there are two time-varying components $\bar{u}'$ and $\bar{u}''$ which may get mixed up. For instance, if we would increase the spatial and temporal resolution of the RANS simulation to a level suitable for Direct Numerical Simulation (DNS) the turbulence model would clearly be superfluous. So with increasing resolution in space and time the RANS model tends to have too much damping in an unsteady flow due to the turbulence model which has been constructed to account for all fluctuations. The usual argument is that when $\bar{u}'$ is characterized by low frequencies distinct from the high-frequency oscillations contained in $\bar{u}''$, in other words when $\bar{u}'$ describes a low-frequency periodic motion and $\bar{u}''$ the turbulence, RANS can still do a fair job in unsteady flows. The periodic shedding phenomenon occurring in cavitation seems to be a case in point. But we can hardly expect grid-independent solutions with unsteady RANS and it is therefore important to check the extent of the influence of spatial and temporal resolution on the results.

Apart from this fundamental issue of the meaning of unsteady RANS, there is also the question: can the same turbulence model be used in a cavitating flow as in a non-cavitating flow? Cavitation and turbulence are likely to have an effect on each other. However, these interaction effects are highly complex and as yet not well understood. Therefore clear-cut rules for adjustment of a turbulence model for cavitation effects are not readily available. Nevertheless Coutier-Delgosha *et al.* [5] have proposed to reduce the eddy viscosity level where vapour appears. And this route has been followed by others [6,7], claiming that only then an unsteady cavitation behaviour more or less corresponding with experiments can be obtained. We can confirm that the proposed correction is a strong stimulant of unsteadiness but it seems an ad-hoc proposal, lacking physical background. This seems to be confirmed in recent work by Bensow [8], comparing the eddy viscosity in RANS and DES simulations of the same flow problem. In the present paper all results are based on the application of the k-ω SST turbulence model in its original form without modification. As will be shown, this does not prevent unsteady behaviour of the cavity to occur.

3 FOIL, GRIDS AND COMPUTATIONAL SETTINGS

We have chosen the NACA0015 foil at 6 degrees angle-of-attack for our numerical studies. The shape of this symmetric foil with a thickness-to-chord ratio of 0.15 is given by an analytical expression [9], yielding a finite thickness at the tail. Instead of modifying the shape so as to obtain a pointed tail, we have just rounded the tail, while maintaining the original chord length.

With a chord length $c=0.20\ m$, the foil was positioned in the middle of a laterally restricted channel of $0.57\ m$ height. The length of the computation domain amounted to 7 chord lengths, from two chords ahead of the leading edge to 4 chords behind the trailing edge. The foil was rotated about its centre of gravity (located at 0.3086 chord behind the leading edge) to an incidence angle of 6 degrees.

A uniform inflow speed $U_\infty=6\ m/s$ was chosen at the inlet plane, while the pressure was prescribed on the outlet. This outlet pressure p is also the reference pressure for the cavitation number σ. On the foil surface no-slip and impermeability conditions were imposed, but on the top and bottom walls free-slip conditions. The fluid properties were chosen as $\rho_l = 998\ kg/m^3$ and $\rho_v = 0.024\ kg/m^3$; $\mu_l = 1.02x10^{-3}\ kg/ms$ and $\mu_v = 1.002x10^{-5}\ kg/ms$. The Reynolds number based on chord length, inflow speed and the kinematic viscosity of the liquid (water) is $Rn=1.2x10^6$.

Five grids were prepared with variable density but of the same lay-out, *viz*. an O-grid embedded in an H-grid. Three grids are geometrically similar and are the same as those used in [1]; two extra grids were made which have extra resolution in the region covering the cavity. The number of grid cells varies as 27808 (G1), 62568 (G2), 111232 (G3), 131736 (G4) and 145602 (G5). The number of cell edges on the foil surface are 234 (G1), 351 (G2), 468 (G3), 500 (G4) and 596 (G5), respectively. An impression of the coarsest grid near the foil can be obtained from Figure 1.

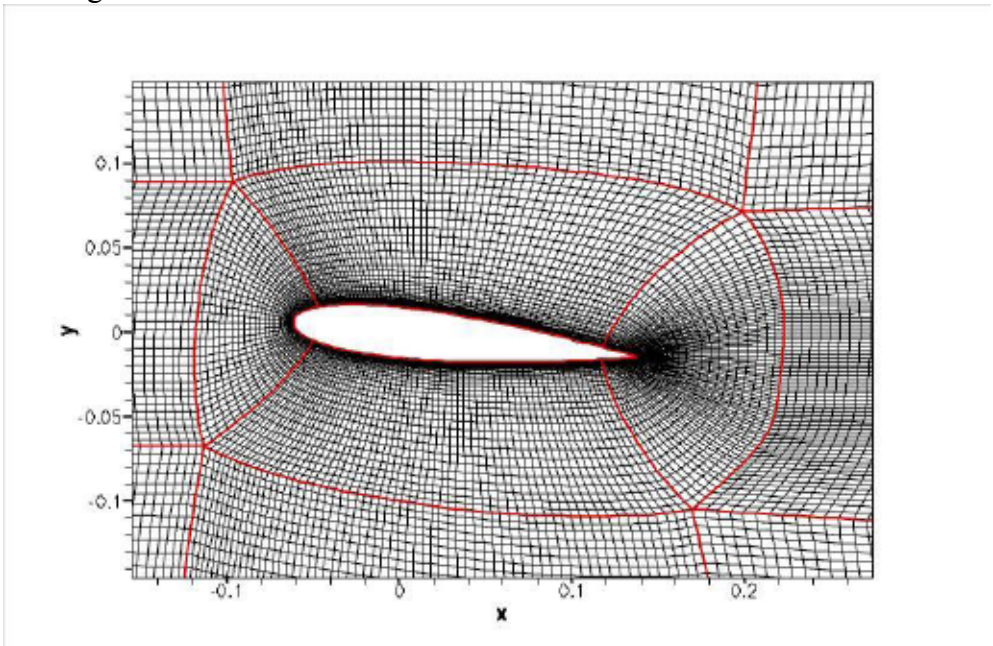

Figure 1: Coarsest grid G1 in the vicinity of the foil

All grids permit full near-wall resolution; the use of wall functions was deliberately avoided. As mentioned before, the k-ω SST turbulence model has been used for all computations reported here.

4 RESULTS

Extensive experimental work on the NACA0015 foil has been done by the groups of Arndt, Keller and Tsujimoto and in Kjeldsen & Arndt [10] an overview diagram of the cavitation behaviour has been given, reproduced here in Figure 2. This will serve as a reference while discussing the results of our numerical simulations. The diagram shows that inception occurs somewhat below the Cp_{min} curve, and the various types of cavitation (bubble, patch, sheet and super cavitation) are indicated. In addition three regions I, II and III are marked to distinguish different dynamic behaviour. Lines of constant cavity length (relative to the chord) are drawn as a reference, representing the result of linearised cavitation theory which concludes that l/c is proportional to α/σ (α is the angle of attack). The same linearised theory gives $l/c=0.75$ as a border beyond which no steady solution exists until the supercavitation stage is reached.

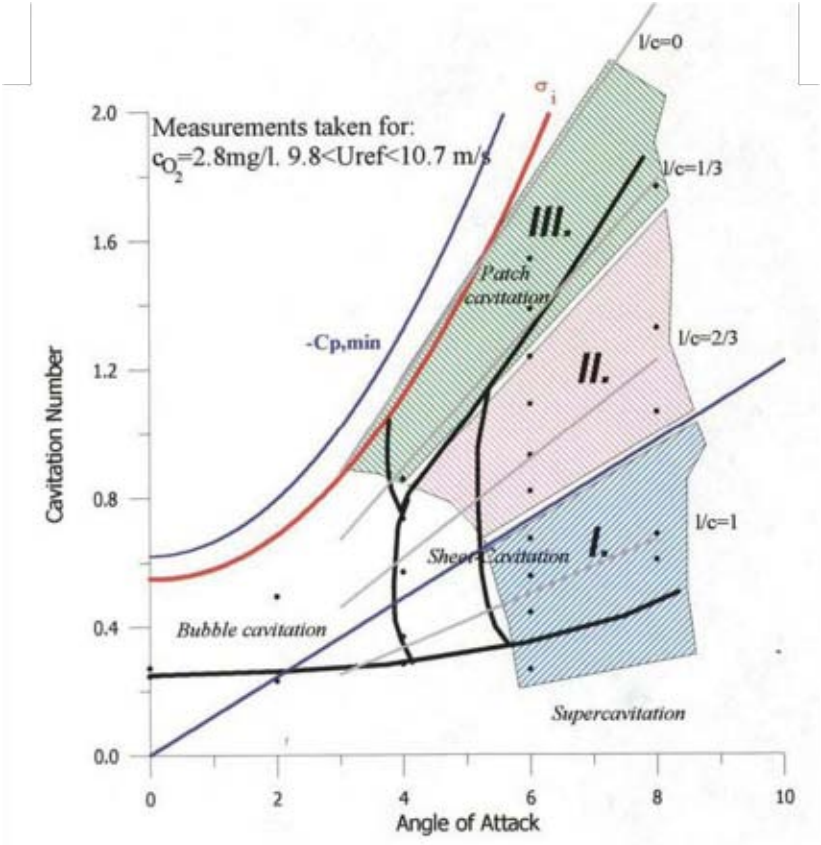

Figure 2: Cavitation behaviour of the NACA0015 foil as a function of cavitation number and angle-of-attack (from Kjeldsen & Arndt [10])

4.1 Steady flow regime

In our RANS simulations we have found a minimum pressure on the foil at 6 degrees incidence in the non-cavitating flow of Cp_{min} = -2.08, which fits nicely in Figure 2, considering that the tunnel height-to-chord ratio is 2.34 in the experiments and 2.85 in our computations. Noteworthy is also the absence of boundary layer separation in the non-cavitating flow.

As soon as the cavitation number σ falls below $-Cp_{min}$ the source term of the evaporation model (see equations (2) and (3)) is activated and phase change starts. Static or thermal delay (as apparently occurs in the experiments summarized in Figure 2) is not part of the model, although it could easily be added if required. So once the flow coming from the stagnation region on the nose of the foil and passing over the suction side reaches the location of $Cp = -\sigma$ vapour production starts, but as the pressure coefficient rises again above $-\sigma$ a little further downstream condensation is activated and vapour will be destroyed. So σ has to be distinctly below $-Cp_{min}$ to "see" any cavitation, in other words to have something corresponding with detection of inception by the naked eye in an experiment.

Evaporation comes with a strong expansion and a change of the pressure. The fluid has to make way to accommodate the expansion and streamlines adjust correspondingly. These effects are connected: the pressure rises (relative to its value in non-cavitating flow) where the cavity starts to form, it decreases where the cavity reaches maximum thickness and rises again when the streamlines bend back to the foil at the closure of the cavity. Correspondingly, the streamline curvature is first reduced, then increased and then decreased again relative to the streamline curvature in the non-cavitating flow (which is only slightly less than the curvature of the foil surface).

The change of the pressure distribution on the foil is illustrated in Figure 3 for $\sigma=1.8$ and for two mass transfer models. Notice that the coordinate on the horizontal axis has its origin at the centre of gravity of the foil, *i.e*. at *0.3086c* from the leading edge. For both models the pressure starts to deviate from the wetted flow pressure as soon as the $Cp=-\sigma$ barrier is passed. Notice that even in the cavitating flow predictions the pressure coefficient stays well below $-\sigma$, which is necessary because evaporation would stop if the pressure would not go below the vapour pressure (as the source term formulation in equation (3) indicates). For Sauer's model the pressure coefficient goes further below $-\sigma$ than for the alternative Kunz model. This is caused by the slower *rate* of evaporation in Sauer's model, which is considered by the author to be the more realistic one.

The change of the pressure field brings about an increase of the adverse pressure gradient close to the tail of the cavity as evidenced by Figure 3, and when strong enough it will induce flow separation. If the flow re-attaches to the foil further downstream (as it does in the given circumstances) a closed separation bubble is established with a recirculating flow inside. Recalling that no boundary layer separation occurred in the non-cavitating flow, the separation is cavitation-induced. And once it has appeared – which happens in our calculations at about $\sigma=1.9$ – there is a region with *reversed flow*, *viz*. the lower part of the separation bubble. This should not be called a re-entrant jet if the latter is understood as a liquid stream coming from the external flow, curling around the cavity tail and then penetrating underneath the cavity [2].

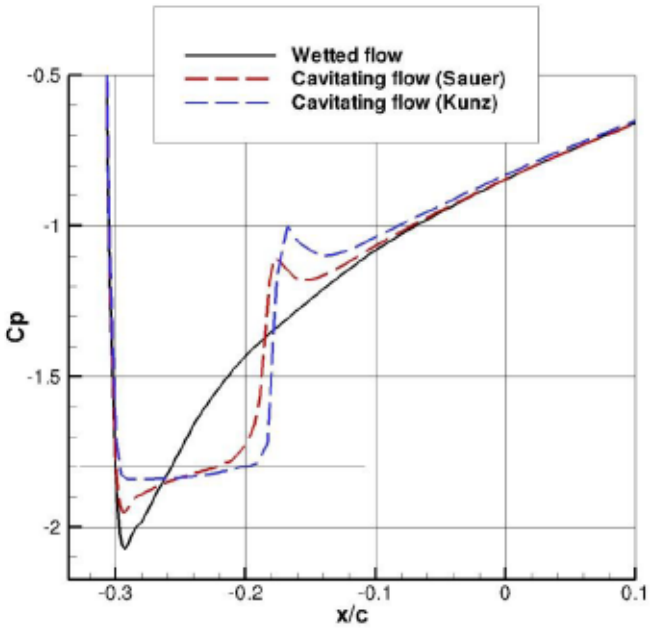

Figure 3: Comparison of pressure distribution on forward part of suction side in wetted flow and cavitating flow (σ=1.8) for two mass transfer models

Reduction of the cavitation number σ leads to growth of the size (length and thickness) of the cavity as well as of the flow re-circulation zone. The increase of the cavity length with decreasing σ is practically linear, which is in accordance with observations (see Fig. 13 in [1]) and reasonably fitting with the linearised theory prediction $l \propto \sigma^{-1}$. For the developed but more or less steady partial cavity the flow is as schematically drawn in Figure 4. We see the shape of the cavity represented by a red line (an iso-line for the vapour volume fraction) and a set of streamlines to represent the underlying flow (notice that the vertical scale has been exaggerated). This picture has some remarkable features, especially for those who are familiar with cavitation simulations based on potential flow assumptions:

- The liquid-vapour interface is not everywhere a material surface, i.e. not everywhere aligned with the flow. This is particularly evident at the tail of the cavity, but it is also true at the front end. Notice the strong convergence of streamlines near the cavity tail, needed to compensate the huge change in fluid density.
- Because the flow is steady, the flow re-circulation zone is bordered by the streamline connecting the separation point and the re-attachment point. We see that the cavity partly overlaps this zone, implying that the flow in the zone is in a continuous process of evaporation and condensation: vapour is generated, travels with the flow and then condensates. While the cavity is stationary, the vapour is in motion.
- Another part of the cavity occurs in the flow field outside the separation bubble. Also here vapour is travelling while the cavity keeps a position stationary to the foil.
- The cavity is on top of the separating shear layer and its tail stays well apart from the foil surface.

- The streamline pattern is different from the classical re-entrant jet flow model, the latter having a liquid stream curling around the cavity tail as a distinct feature.

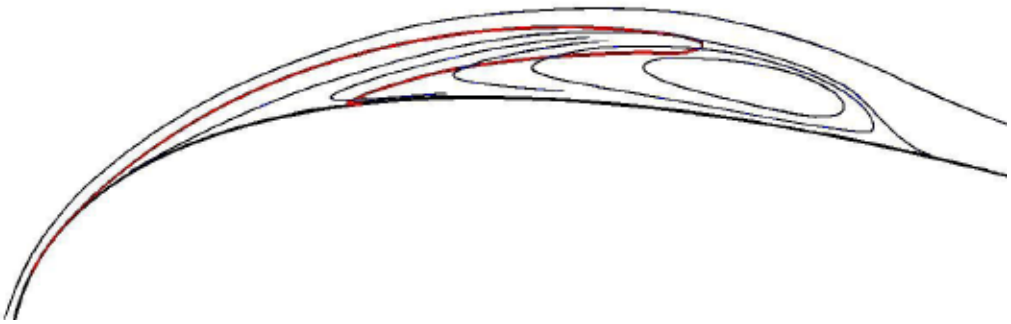

Figure 4: Cavity outline and streamlines for a stable partial cavity

As is physically understandable and as equation (5) indicates, there is no net source left in equation (2) if the cavity is steady. It does not mean that all sources vanish; our results clearly show sources, particularly at the forward part of the cavity, and compensating sinks, concentrated in the tail part. So instead of a cavity filled with the same vapour over time, there is a continuous creation and destruction of vapour even under steady flow conditions.

The effect of spatial resolution on the results is moderate. The total vapour volume tends to decrease slightly with increasing grid refinement, the liquid-vapour interface getting sharper where it is more or less aligned with the flow.

In our calculations the cavity is steady for small cavity lengths. Referring to Figure 2, the experiments show patch cavitation for these small cavity lengths, i.e. a coherent cavity with small fluctuations. Tulin [11] has called this a cavity which is "steady in the mean". The fluctuations of small partial cavities observed in an experiment are presumably due to turbulence or to slight perturbations of the flow conditions in the experimental facility.

4.2 Cavitation compliance

The trend in the steady regime is that with decreasing cavitation number the vapour volume increases: $-d\mathcal{V}/d\sigma > 0$, if $\mathcal{V}$ denotes the total vapour volume. This is related to the concept of *cavitation compliance* ($K = -\rho_l \, d\mathcal{V}/dp$), a measure for the change of cavity volume with decreasing pressure. If the pressure in K is assumed to be the far-field pressure, K is directly proportional to $-d\mathcal{V}/d\sigma$. The computational results indicate that $-d\mathcal{V}/d\sigma$ rises to a maximum at about $\sigma=1.5$ and then decreases for lower σ. Consequently there is a gradual loss of cavitation compliance beyond $\sigma=1.5$.

That cavitation compliance possibly has a role in the onset of dynamic behaviour can be made plausible by a simplified analysis as follows. From the definition of the compliance K we derive

$$K\frac{dp}{dt} = -\rho_l \frac{d\mathcal{V}}{dt},$$

if K is assumed not to vary with time. Differentiating with time yields

$$K\frac{d^2p}{dt^2} = -\rho_l \frac{d^2\mathcal{V}}{dt^2}.$$

But a fluctuating cavity volume radiates an acoustic pressure of which the lowest harmonic is proportional to the second time derivative of the volume:

$$p = A\frac{d^2\mathcal{V}}{dt^2} \qquad (A > 0).$$

If the pressures in the last two equations are considered the same, we arrive at

$$\frac{d^2p}{dt^2} + \frac{\rho_l}{AK}p = 0$$

For $K>0$ this equation leads to $p \sim e^{i\omega t}$, a harmonic oscillation with frequency $\omega = \sqrt{\rho_l/AK}$, but for $K<0$ it allows exponential growth solutions: $p \sim e^{at}$, with $a = \sqrt{-\rho_l/AK}$.

In the analysis given above, p seems a near-field rather than a far-field pressure. Looking for a quantity representing more or less a near-field pressure, the lift coefficient comes to mind. If the pressure on the suction side decreases, the lift coefficient is expected to increase. So for positive K one expects $d\mathcal{V}/dC_L > 0$. This is the case for $2.1<\sigma<1.9$, and in a potential flow this would be explained as a gain of lift due to a slight increase of the effective camber of the foil by the presence of the cavity. But below $\sigma=1.9$ C_L drops quickly with lowering σ. This is due to the appearance of flow separation; the foil gets stalled. The trend for C_L is comparable with the change of static lift with angle-of-attack in non-cavitating flow: the lift grows with increasing α, but it breaks down on the appearance of flow separation. In passing, we observe that in non-cavitating flow the NACA0015 foil is a trailing-edge stalling foil (separation occurs first at about $\alpha=8^o$ in the vicinity of the trailing edge), but in cavitating flow a leading-edge stalling foil. These global trends are plotted in Figure 5 (CLo being the lift in non-cavitating flow). It shows that $d\mathcal{V}/dC_L < 0$ for the developed cavity but tends to 0 on approaching the unsteady regime.

Whether a loss of cavitation compliance is the cause or a symptom of the onset of dynamic behaviour can unfortunately not conclusively be decided.

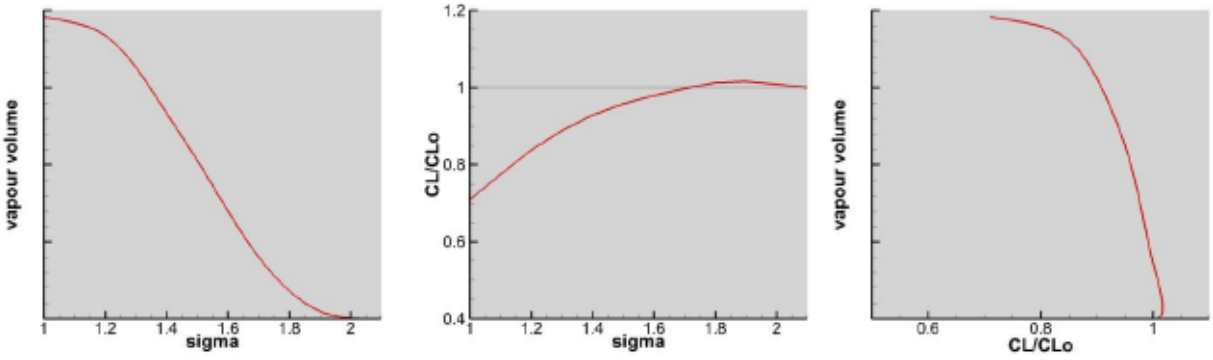

Figure 5: Global trends in variation of cavity volume and lift with σ in steady flow

4.3 Oscillatory behaviour

Our computations indicate that oscillatory behaviour starts near σ=1.2. The cavity has grown then to about 1/3 of the chord and the flow re-attachment point (aft end of separation bubble) has moved beyond mid-chord. As noted above, on approaching the onset of dynamic behaviour the total vapour volume gets rather insensitive to a change in C_L. The oscillation is not immediately accompanied with shedding of vapour clouds, although there is shedding of vorticity. We rather observe a "breathing" cavity in the initial phase of unsteady behaviour. So there are vapour volume oscillations accompanied with lift force oscillations, the lift variation having a phase lag relative to the vapour volume variation. Shedding of vapour clouds occurs for still lower values of the cavitation number.

The initial oscillatory behaviour can de characterized as follows (we describe the results at σ=1.2). While in the steady regime (with short partial cavities) an increase in the cavity length is always accompanied with an increase in the total vapour volume, now there is evidence of the opposite tendency: a reduction of vapour concentration and a thinner cavity while it is elongating. Perhaps this is related to a change of the tail part of the cavity, being coincident with the separating shear layer and clearly away from the foil surface, from attached sheet to shear cavitation. Anyway, thinning of the cavity is directly linked with further penetration of liquid underneath the cavity. When the length of the cavity and the extent of the separation bubble are at a maximum, the lift force is also at its maximum but then starts to drop while the vapour volume continues to decrease, the cavity retreats and the separation bubble shrinks. Lift reduction implies the shedding of vorticity (connected with the loss of circulation around the foil) and while this vorticity travels over the suction side it first induces separation at the tail of the foil and upon passing the trailing edge a counter rotating vortex is shed there. A pair of counter-rotating vortices is then traveling downstream and the cavity starts to grow again.

We observe that the lift reaching a maximum when the separation bubble is at maximum extent is in great contrast with the static lift behaviour.

Shedding of cavitation clouds starts in our calculations at σ=1.1. A sequence of pictures illustrating the cavitation behaviour during one cycle is shown in Figure 6. The main difference with the results at σ=1.2 is that the separation bubble now covers the complete suction side of the foil during part of the oscillation and is subsequently swept from the foil so that the flow is practically free of separation during another part of the cycle. In other words, shedding is related to a dynamic stall process.

Starting from the moment that the cavity is smallest (Figure 6a), its length and volume grow rapidly (Figure 6b-d). Because the cavitation-induced separation bubble grows in length and thickness, the distance of the cavity tail to the foil surface grows. While the cavity length is between 0.5c and 0.65c (the flow re-attachment point being between 0.6c and 0.75c), we see a thin layer of liquid penetrating under the forward part of the cavity (Figure 6d-f). Some would immediately call this a re-entrant jet, but seeing nothing of the flow features of the classical re-entrant jet flow, but rather a process of thinning of the cavity with as a consequence the appearance of more liquid under the cavity, the author is reluctant to follow this interpretation (see also [2]). Although a weak spot in the cavity occurs close to the forward end of the cavity it does not break there. Instead we see a break in the cavity appearing above about mid chord a few instants later (Figure 6g). The flow reattachment point (end of the

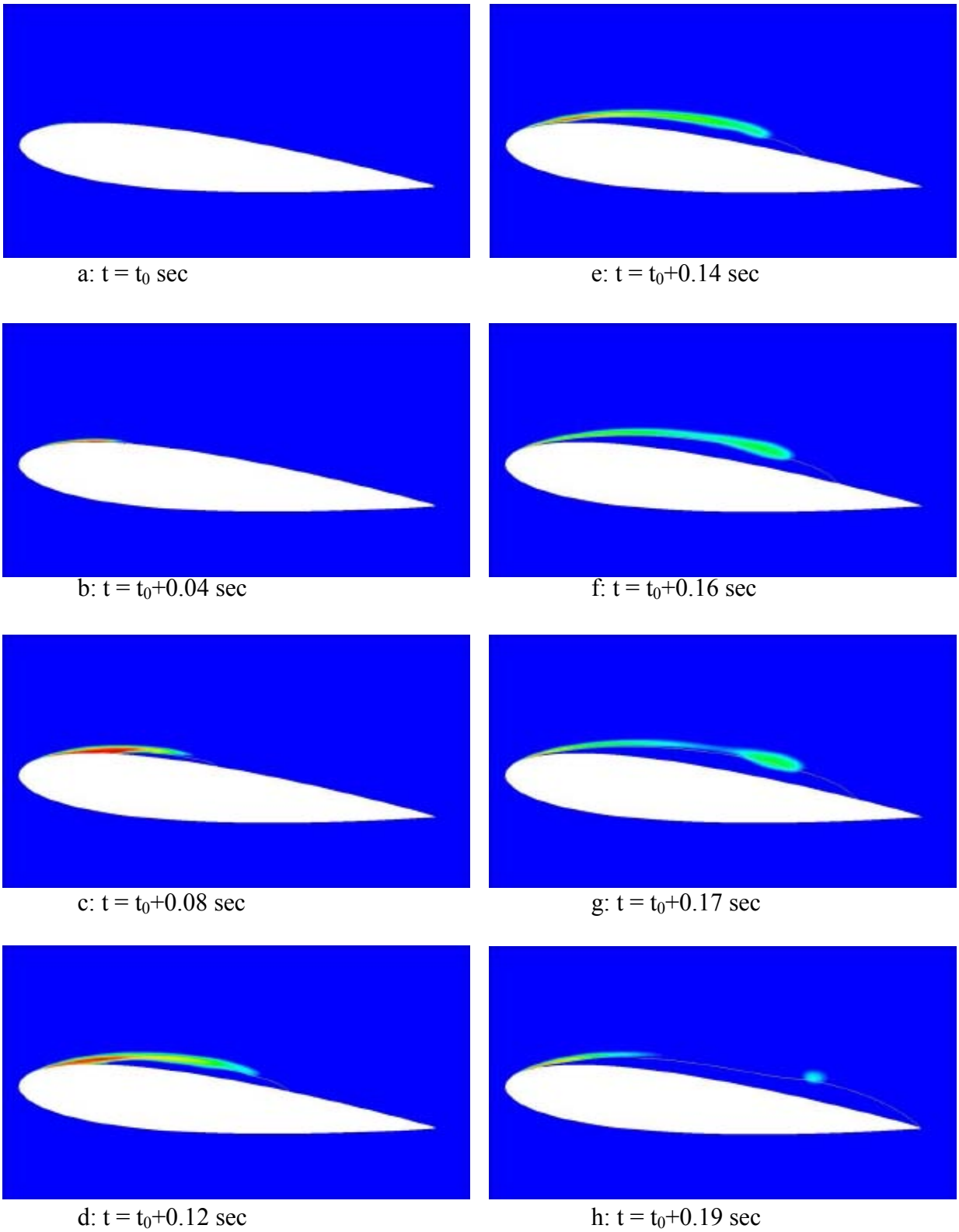

a: $t = t_0$ sec

e: $t = t_0$+0.14 sec

b: $t = t_0$+0.04 sec

f: $t = t_0$+0.16 sec

c: $t = t_0$+0.08 sec

g: $t = t_0$+0.17 sec

d: $t = t_0$+0.12 sec

h: $t = t_0$+0.19 sec

Figure 6: Snapshots of periodic cavity shedding at σ=1.1; cycle period ~0.28 sec

separation bubble) has then not yet reached the trailing edge. While the separation zone grows to the trailing edge, the forward part of the cavity retreats and the shed cloud – which is at the centre of a clockwise-rotating vorticity region - moves downstream and collapses near a chord position of 0.2c ahead of the trailing edge (Figure 6h). Just before this collapse, the lift force takes its maximum value which is in excess of the lift in non-cavitating flow. Although the cavitation in the shed cloud has disappeared, the vorticity is still there and just before that vorticity reaches the trailing edge we see the direction in which the flow leaves the trailing edge changing (more upward inclination). The lift is meanwhile dropping quickly. Subsequently, when the cavity has reduced to minimum size, flow reattachment occurs just aft of the cavity, causing the separation bubble to split into two parts, and while the cavity starts growing again the flow detachment point of the rear part of the separation region quickly moves towards the trailing edge. Just before it has reached the trailing edge the lift force is at a minimum value. A strong reaction at the trailing edge follows: a counter-clockwise rotating vortex is shed from the trailing edge, implying rising lift. While the separation zone is swept off the foil, a series of clockwise-rotating vorticity clouds is passing over the suction side. Exactly this feature is also reported by McCroskey [12] to happen in dynamic stall of an airfoil under forced oscillations. Evidence of these vortices is further given in LES simulations reported by Arndt and Song [13,14]. This is presumably the vorticity shed due to lift reduction.

The lift variation is not just a matter of trailing edge flow conditions, the position of the stagnation point on the nose of the foil is also changing. While the separation is swept from the foil the angle of attack is at a minimum.

Lowering the cavitation number to σ=1.0, gives similar results as for σ=1.1, but the amount of vapour is greater and the dynamic process is getting more violent. A much bigger cloud is being shed, the cavity breaking apart when the closure point of the separation bubble has practically reached the trailing edge of the foil. The collapse occurs when the cloud is above the trailing edge. The counter-clockwise rotating vortex shed from the trailing edge gets filled with vapour at its core and this cavity grows while the shed cloud above the trailing edge collapses. The oscillation frequency is not much affected. CL drops before vapour volume drops. A short period of negative lift is now part of the oscillation cycle.

4.4 Re-entrant jet or not?

As we have observed above, from the instant that the cavity volume (not its length!) reaches a maximum the cavity tends to get thinner and more liquid is appearing under the cavity as a consequence. This seems to be a condensation phenomenon, rather than a re-entrant jet. For a re-entrant jet one would expect the vapour-liquid interface to travel with local fluid speed, but this is not generally the case. In steady flow conditions this is immediately clear: the interface is stationary while the fluid moves beneath the cavity in upstream direction. But it holds also in dynamic conditions, where the interface may be moving faster than the fluid itself. It is the author's impression that what is called *re-entrant jet behaviour* is a strong visual illusion: the human brain tends to interpret the motion of the interface as the motion of the fluid. Sato[15] has given experimental corroboration to this viewpoint. He and his student Shimojo studied dynamic cavitation in a convergent-divergent nozzle and have cast doubt on the occurrence of the re-entrant jet phenomenon in the

following remark: "*The mechanism of this advancing motion remains to be completely solved whether the motion is caused mainly by the re-entrant jet or mainly by the propagation of bubble collapses due to pressure. For the present study, the latter mechanism <…> appears to be main or dominant at the last stage of the re-entrant motion because the detailed observation near the nozzle throat indicates that the collapse of bubbles propagates upstream at some speed while the translational speed of bubbles seems to be very small*".

4.5 Vapour volume versus lift

We have seen in Figure 5 how the vapour volume behaves against the static lift under changing cavitation number. Figure 7 gives an example of vapour volume against lift for constant σ in dynamic conditions. For σ=1.2 (Figure 7a) we see a closed loop (representing an almost harmonic oscillation) instead of a curve spiraling to a single point if the flow would become steady. During the greater part of the cycle $d\mathcal{V}/dC_L > 0$. It is a clockwise loop: the lift variation has a phase lag relative to the vapour volume variation.

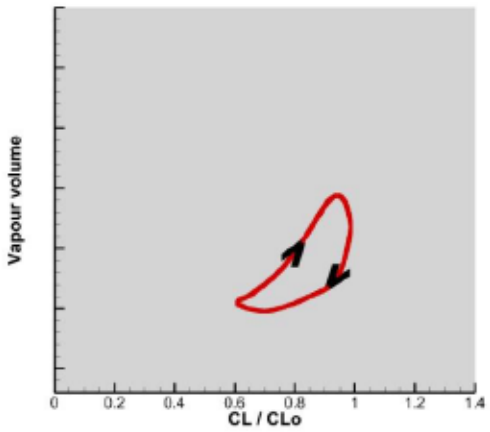

Figure 7a: Cavity volume versus lift for σ=1.2

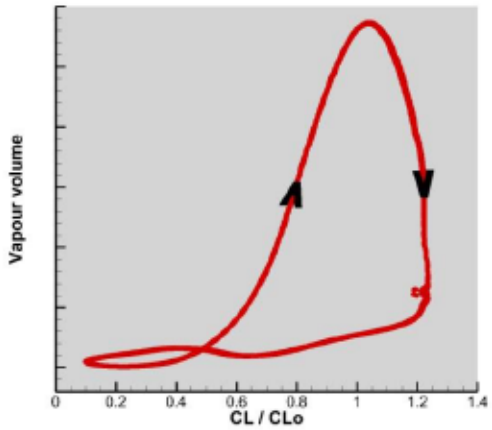

Figure 7b: Cavity volume versus lift for σ=1.1

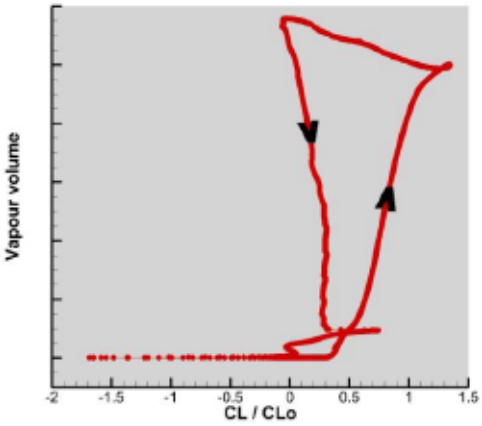

Figure 7c: Cavity volume versus lift for σ=1.0

Figure 7b for σ=1.1 is plotted on the same scale as Figure 7a, clearly bringing out that the oscillation amplitude is growing with decreasing cavitation number. The lift exceeds the wetted-flow lift significantly over a part of the cycle. This is typical for dynamic stall processes [12]. The behaviour at σ=1.1 (Figure 7c) requires an adjustment of the scale on the horizontal axis of the plot. The loop is now traversed in counter-clockwise direction.

4.5 Oscillation frequency

The dominant frequency of the periodic cavity oscillation varies in our results somewhat with σ and with spatial/temporal resolution but is nevertheless within a narrow band between 3.5 and 4 Hz. The Strouhal number $Str=fc/U$ is then in the range $0.117<Str<0.133$. How does this compare to other sources of information? Strikingly, there is no uniformity in the Strouhal number as it is reported for partial and transitional cavity oscillations on foils, either based on experiments or on numerical simulations. As a matter of fact, leaving apart the high Strouhal numbers found for small partial cavities, the oscillation frequencies for well-developed cavities (mean cavity length between 0.5c and 1.2c) fall in two categories, either in the range $0.12<Str<0.15$ or at roughly the double frequency $0.25<Str<0.30$. For instance, Wade and Acosta [16] report based on their early experiments Strouhal numbers in the range of 0.07 to 0.14. Sato *et al.* [17] found later $0.13<Str<0.15$ and similar results were reported by Watanabe *et al.* [18]. But lots of other experiments indicate a frequency which is roughly twice as high, $0.25<Str<0.3$. Focussing on the NACA0015 foil, we are in the happy circumstances that extensive measurements have been made in three cavitation tunnels (Minnesota, Obernach and Osaka) by Arndt, Keller and Tsujimoto in close cooperation. Arndt [19] has recently given a summary of the outcome in an invited lecture during the last Cavitation Forum. But also here a division appears, the Obernach data falling in the high frequency range, the Minnesota and Osaka data in the low frequency range. Actually, Arndt *et al.* [14] indicate that the two frequencies can occur in the same experiment, but not simultaneously.

On the computational side we can also mention a few results for the NACA0015 foil. Schnerr *et al.* [20] report $Str=0.133$ based on results of their Euler code CATUM, Li *et al.* [6] report 3.5 Hz or $Str=0.117$ using the RANS model of FLUENT and computing exactly the same configuration as we have done. But LES simulations tend to show frequency spectra with a higher peak near $Str=0.25$-0.30 than at $Str=0.12$-0.15 [21,22].

This puzzling issue of the oscillation frequency is to be sorted out further. An extra complication is that in a closed-circuit experimental facility system instabilities may interfere. Duttweiler and Brennen [23,24] but also Kawakami *et al.* [25] have reported on the possible interference of facility dynamics with cavitation dynamics. And one may wonder whether numerical simulations are in this respect free of domain-size influences. Equation (4) expresses that the cavitation source function is directly proportional to the divergence of the velocity field. So a fluctuating source gives rise to mass flow oscillations. Since the mass flow rate at inflow is constant (by the boundary conditions) the mass flow rate at outflow must be varying in time. There the pressure is held fixed and pressure fluctuations due to the oscillating source, traveling with infinite signal speed (incompressible liquid), are "cushioned" close to the outlet. Is there a possible feed-back?

5 CONCLUSIONS

In this paper we have explored the capabilities of the single-fluid RANS model for cavitation simulations for a 2D foil, specifically the NACA0015 foil at 6 degrees angle-of-attack. The focus has been on the transition from steady to dynamic behaviour of the partial cavity. The following conclusions are drawn:

- The single-fluid model in combination with the RANS equations for the simulation of cavitation in flowing liquids is able to give realistic results for the behaviour of a partial cavity on a 2D foil. It is able to predict the change from steady to oscillatory behaviour and is informative on the flow behaviour in steady as well as unsteady conditions.
- It is widely accepted that a re-entrant jet determines the onset of dynamic behaviour of the cavity. Also in the results presented here there is a reversed flow and a clear indication of liquid penetrating under the cavity. Yet, no evidence has been found of the classical re-entrant jet flow.
- The onset of unstable cavity behaviour can perhaps be associated with a loss of cavitation compliance, a measure for the cavity volume to grow with decreasing pressure. At least the instability is initiated when the length of the cavity increases while the cavity volume decreases.
- The periodic oscillations following the appearance of instability could be convincingly shown to be a dynamic stall phenomenon. When shedding of vapour clouds is observed, the cavitation-induced separation bubble grows until it covers the complete suction side of the foil and is subsequently swept from the foil in periodic succession.

NOMENCLATURE

c	chord length
C_L	lift coefficient
C_{Lo}	lift coefficient in non-cavitating flow
Cp	pressure coefficient
K	cavitation compliance
p	pressure
Rn	Reynolds number
Str	Strouhal number based on chord
$\mathcal{V}$	total vapour volume
α	angle of attack
α_v	vapour volume fraction
ρ	density of mixture fluid
ρ_l	liquid density
ρ_v	vapour density
σ	cavitation number

REFERENCES

[1] M. Hoekstra and G. Vaz, "The partial cavity on a 2D foil revisited", *7th Int. Symp. on Cavitation*, Ann Arbor, Michigan, USA (2009).

[2] M. Hoekstra, "The myth of the re-entrant jet", *3rd Int. Cavitation Forum*, University of Warwick, UK (2011).

[3] J. Sauer, "Instationär Kavitierende Strömungen – Ein Neuse Modell, Basierend auf Front Capturing (VoF) und Blasendynamik", *PhD University of Karlsruhe*, Germany (2000).

[4] G.H. Schnerr and J. Sauer, "Physical and numerical modeling of unsteady cavitation dynamics", *4th Int. Conf. on Multiphase Flow*, New Orleans, USA (2001).

[5] O. Coutier-Delgosha, R. Fortes-Patella and J.L. Reboud, "Evaluation of the Turbulence Model Influence on the Numerical Simulations of Unsteady Cavitation", *J. Fluids Engineering*, **125**, 38-45 (2003).

[6] D.Q. Li, M. Grekula and P. Lindell, "A modified SST k-ω turbulence model to predict the steady and unsteady sheet cavitation on 2D and 3D hydrofoils", *7th Int. Symp. on Cavitation*, Ann Arbor, Michigan, USA (2009).

[7] E. Sorgüven and G.H. Schnerr, "Modified k-ω model for simulation of cavitating flows", *Proc. Appl. Math. Mech.* **2**, 386-387 (2003).

[8] R.E. Bensow, "Simulation of unsteady cavitation on the Delft twist11 foil using RANS, DES and LES", *2nd Int. Symp. on Marine Propulsors*, Workshop 1, Hamburg (2011).

[9] I. A. Abbott and A. E. von Doenhoff, *Theory of Wing Sections,* Dover Publications, New York (1958).

[10] M. Kjeldsen and R.E.A. Arndt, "Spectral characteristics of sheet/cloud cavitation", *J. Fluids Engineering*, **122**, no. 3, 481-487 (2000).

[11] M.P. Tulin, "On the theory and modeling of real cavity flows", *5th Int. Symp. on Cavitation*, Osaka, Japan (2003).

[12] W.J. McCroskey, "The phenomenon of dynamic stall", *NASA Technical Memorandum* (1981).

[13] R.E.A. Arndt, C.C.S. Song and Q. Qin, "Experimental and numerical investigations of cavitating hydrofoils", *22nd IAHR Symp. on Hydraulic Machinery and Systems*, Stockholm, Sweden (2004).

[14] R.E.A. Arndt, C.C.S. Song, M. Kjeldsen, J. He and A. Keller, "Instability of partial cavitation: a numerical/experimental approach", *23rd Symp. on Naval Hydrodynamics*, Val de Reuil, France (2000).

[15] K. Sato and S. Shimojo, "Detailed observations on a starting mechanism for shedding of cavitation cloud", *5th Int. Symp. on Cavitation*, Osaka, Japan (2003).

[16] R.B. Wade and A.J. Acosta, "Experimental observations on the flow past a plano-convex hydrofoil", Transactions ASME, Jnl. Basic Engineering, 88, no.1 (1966).

[17] K. Sato, M. Tanada, S. Monden and Y. Tsujimoto, "Observations of oscillating cavitation on a flat plate hydrofoil", *4th Int. Symp. on Cavitation*, California Institute of Technology, Pasadena, California, USA (2001).

[18] S. Watanabe, Y. Konishi, I. Nakamura and A. Furukawa, "Experimental analysis of cavitating behaviour around a Clark Y hydrofoil", *WIMRC 3rd Int. Cavitation Forum*, University of Warwick, UK (2011).

[19] R.E.A. Arndt, "Some remarks on hydrofoil cavitation", *WIMRC 3rd Int. Cavitation Forum*, University of Warwick, UK (2011).
[20] G.H. Schnerr, S. Schmidt, I. Sezal and M. Thalhammer, "Shock and wave dynamics of compressible liquid flows with special emphasis on unsteady load on hydrofoils and on cavitation in injection nozzles", *6th Int. Symp. on Cavitation*, Wageningen, The Netherlands (2006).
[21] S.E. Kim, "A numerical study of unsteady cavitation on a hydrofoil", *7th Int. Symp. on Cavitation*, Ann Arbor, Michigan, USA (2009).
[22] N.X. Lu, R.E. Bensow and G. Bark, "Grid resolution effects in simulating unsteady sheet cavitation", in *Large Eddy Simulation of Cavitating Flow on Hydrofoils*, PhD, Chalmers University of Technology, Gotheburg, Sweden (2010).
[23] M.E. Duttweiler, S.E. Schell and C.E. Brennen, "The effect of experimental facility dynamics on a cavitation instability", *ASME Fluids Engineering Division Summer Meeting*, Boston Massachusetts (2000).
[24] M.E. Duttweiler and C.E. Brennen, "Surge instability on a cavitating propeller", *4th Int. Symp. on Cavitation*, California Institute of Technology, Pasadena, California, USA (2001).
[25] D.T. Kawakami, A. Fuji, Y. Tsujimoto and R.E.A. Arndt, "An assessment of the influence of environmental factors on cavitation instabilities", *J. Fluids Engineering*, **130**, (2008).